Pure Appl. Geophys. 175 (2018), 3539–3553

https://doi.org/10.1007/s00024-018-1867-0

Pure and Applied Geophysics

PSO (Particle Swarm Optimization) for Interpretation of Magnetic Anomalies Caused by Simple Geometrical Structures

Khalid S. Essa[1] and Mahmoud Elhussein[1]

Abstract—A new efficient approach to estimate parameters that controlled the source dimensions from magnetic anomaly profile data in light of PSO algorithm (particle swarm optimization) has been presented. The PSO algorithm has been connected in interpreting the magnetic anomaly profiles data onto a new formula for isolated sources embedded in the subsurface. The model parameters deciphered here are the depth of the body, the amplitude coefficient, the angle of effective magnetization, the shape factor and the horizontal coordinates of the source. The model parameters evaluated by the present technique, generally the depth of the covered structures were observed to be in astounding concurrence with the real parameters. The root mean square (RMS) error is considered as a criterion in estimating the misfit between the observed and computed anomalies. Inversion of noise-free synthetic data, noisy synthetic data which contains different levels of random noise (5, 10, 15 and 20%) as well as multiple structures and in additional two real-field data from USA and Egypt exhibits the viability of the approach. Thus, the final results of the different parameters are matched with those given in the published literature and from geologic results.

Key words: Magnetic anomaly, PSO algorithm, the depth, RMS.

1. Introduction

Magnetic anomaly interpretation is significantly important in exploring regions with targets under the surface (Nabighian et al. 2005; Abdelrahman et al. 2009; Ekinci et al. 2014). In addition, it can be applied in hydrocarbon exploration (Abubakar et al. 2015; Ivakhnenkoa et al. 2015), in ores and mineral exploration (Farquharson and Craven 2009; Abedi et al. 2013; Abdelrahman et al. 2016), in engineering applications (Dong et al. 2007), in geothermal activity (Bektas et al. 2007; Nyabeze and Gwavava 2016), in archaeological site investigations (Gündoğdu et al. 2017), in weapon inspection (Davis et al. 2010; Yin et al. 2017), and in hydrological investigations (Al-Garni 2011; Araffa et al. 2015). In general, most of magnetic interpretation methods are carried out assuming the subsurface structures are simple geometrical shapes (for example spheres, horizontal cylinders, thin sheets, faults) buried at different depth generated by different minerals, ore bodies and oil deposit (Abo-Ezz and Essa 2016).

Generally, inversion of magnetic data includes estimating the model parameters (depth, amplitude coefficient and the dip angle) of buried geologic structures. Numerous methods have been used to interpret magnetic data such as Werner deconvolution (Ku and Sharp 1983), Euler deconvolution (Thompson 1982) and parametric curves approach (Abdelrahman et al. 2012). In addition, layered-model inversion (Pilkington 2006), gradient methods (Abdelrahman et al. 2003; Essa and Elhussein, 2017a), fair function minimization procedure (Tlas and Asfahani 2011), DEXP (Fedi 2007), linear least squares approach (Abdelrahman et al. 2007; Abo-Ezz and Essa 2016), and simplex algorithm (Tlas and Asfahani 2015) approaches. However, these conventional inversion approaches are that some of them generate large number of invalid solutions because of noise sensitivity, misconception between causative bodies and window sizes. In addition, some of them require initial model parameters that depending on geologic information, utilizing few data points on profile, claim understanding of shape factor and require more time.

These are the disadvantages of above-mentioned conventional inversion methods. For the past two

[1] Geophysics Department, Faculty of Science, Cairo University, P.O. 12613, Giza, Egypt. E-mail: mahmoudelnouishy@yahoo.com

decades, global optimization methods have been used in many areas as an alternative to these geophysical inversion methods such as genetic algorithm (Boschetti et al. 1997; Kaftan 2017), particle swarm optimization (van den Bergh and Engelbrecht 2004; Essa and Elhussein 2017b), differential evolution (Ekinci et al. 2016; Balkaya et al. 2017), simulated annealing (Biswas 2015), ant colony optimization (Colorni et al. 1991; Srivastava et al. 2014) and hybrid genetic-price algorithm (Bresco et al. 2005; Di Maio et al. 2016).

Particle swarm optimization algorithms (PSO) are effective optimization methods for solving difficult problems reliably and accurately. The PSO method is a stochastic developmental computation technique and was first produced by Kennedy and Eberhart (1995). It is primary on the simulation of the plain conduct of birds, fishes and insects in nourishment seeking. In this algorithm, the birds represent the particles or models. Each particle has a location vector which represent the parameters esteem and a speed vector. For example, for a five-dimensional optimization problem, each particle or individual will have a location in five-dimensional spaces which represent a solution (Eberhart and Shi, 2001). The implementations of the particle swarm optimization technique on geophysical data inversion and modeling were carried out (Toushmalani 2013; Peksen et al. 2014; Singh and Biswas 2016; Essa and Elhussein 2017b). Likewise, it is connected to many issues, like machine learning (Juang 2004), model construction (Cedeno and Agrafiotis 2003), biomedical images (Wachowiak et al. 2004), inverse scattering (Donelli et al. 2006), electromagnetic optimizations (Robinson and Rahamat-Samii 2004) and hydrological problems (Chau 2008).

In this study, we applied the PSO algorithm to the inversion of magnetic anomalies over simple causative sources. The model parameters estimated are the depth (z), the location of the origin (x_o), shape factor (S_f), index angle (θ) and the amplitude coefficient (K). The use of this study was demonstrated by different synthetic models without and with different levels of random noise (5, 10, 15, and 20%), multi-models and two real examples. The model parameters estimated values compared with the results of the conventional inversion methods used in previous studies and drilling information. The results obtained from this comparison reveal that our algorithm is more stable and resolvable.

2. Methodology

2.1. Two-Dimensional Magnetic Forward Problem

The general new formula of two-dimensional magnetic anomaly (T) profile for simple-geometric bodies was summed up by Abdelrahman and Essa (2015) after careful investigation of magnetic anomaly expressions of the spheres (Rao et al. 1977; Rao and Subrahmanyam 1988), the horizontal cylinders (Rao et al. 1986) and the thin sheets (Gay 1963) which is described as follows:

$$T(x_i,z) = K\frac{Az^2 + B(x_i - x_o) + C(x_i - x_o)^2}{\left[(x_i - x_o)^2 + z^2\right]^{S_f}}, \quad i = 0,\ 1,\ 2,\ 3,\ldots,N \tag{1}$$

where K is the amplitude coefficient, z is the depth of the buried body, A, B, and C are defined as follows:

$$A = \begin{cases} 3\sin^2\theta - 1 & \text{for a sphere (total field)} \\ 2\sin\theta & \text{for a sphere (vertical field)} \\ -\cos\theta & \text{for a sphere (horizontal field)} \\ \cos\theta & \text{for a horizontal cylinder, FHD of thin sheet,} \\ & \text{and SHD of geological contact (all fields)} \\ \dfrac{\cos\theta}{z} & \text{for a thin sheet and FHD of geological contact (all fields).} \end{cases}$$

$$B = \begin{cases} -3z\sin\theta \\ -3z\cos\theta \\ -3z\sin\theta \\ 2z\sin\theta \\ \\ -\sin\theta \end{cases}, \quad C = \begin{cases} 3\cos^2\theta - 1 \\ -\sin\theta \\ 2\cos\theta \\ -\cos\theta \\ \\ 0 \end{cases},$$

θ is the angle of effective magnetization which is clearly demonstrated by Rao et al. (1973) and Rao and Subrahmanyam (1988) in case of spheres. In addition, for the case of thin sheets and horizontal cylinders is defined by Gay (1965), x_o is the coordinate of the center of the source body, FHD is the first horizontal derivative, SHD is the second horizontal derivative of the magnetic anomaly, respectively, N is the number of data points, and S_f is the shape factor (for sphere $S_f = 2.5$, for horizontal cylinder $S_f = 2$, and for thin sheet $S_f = 1$ (Abdelrahman and Essa 2005).

2.2. Magnetic Inverse Problem

The inversion method in geophysics is an optimization process that finds the model parameters of the buried geologic structures which nicely explains the observed data. The inverse problem solution requires the supposition of an initial model (Lines and Treitel 1984; Zhdanov 2002; Tarantola 2005; Mehanee et al. 2011). A promising initial model could be made by introducing a priori information from geology, drilling or other geophysical techniques (Zhdanov 2002; Mehanee 2014; Mehanee and Essa 2015). The initial model is increasingly polished at every iteration step until a best fit is reached between the estimated and measured data. In every step, the model parameters are changed to get a better fitting between the measured and estimated data. The iteration process is continued until the best model parameters (better data misfit) are executed at the minimum value of the objective function (Eq. 2) $\approx$ zero.

According to the two-dimensional magnetic formula (Eq. 1), the unknown model parameters are the depth (z), the location of the origin (x_o), shape factor (S_f), index angle (θ) and the amplitude coefficient (K).

The particle swarm optimization (PSO) algorithm has been used to solve the inverse problem because it is mathematically robust and numerically stable due to the rapidity of merging fewer operators, and easy to execute because of simplicity of its procedures (Pallero et al. 2018).

To find the best value of the model parameters in a manner that minimizes the differences between the observed field data and the estimated model, we use the following simple objective function:

$$Q = \frac{2\sum_{i=1}^{N}\left|T_i^m - T_i^c\right|}{\sum_{i=1}^{N}\left|T_i^m - T_i^c\right| + \sum_{i=1}^{N}\left|T_i^m + T_i^c\right|}, \quad (2)$$

where N is the number of data points, T_i^m is the measured magnetic anomaly at the point x_i, T_i^c is the estimated magnetic anomaly at the point x_i.

2.3. The Particle Swarm Optimization (PSO)

The particle swarm optimization (PSO) method is a global optimization algorithm proposed by Kennedy and Eberhart (1995). It is relied on the simulation of the apparent behavior individuals (called particles) in nature, for example, bird flocking and fish tutoring. In a PSO algorithm, every particle is a competitor solution identical to a point in M-dimensional space. The calculation is randomly introduced and the particles (initial solutions) are set randomly in the inquiry space of the objective function (He and Guo 2013). The PSO algorithm effectively prompts to a global optimum. The fundamental concept of the PSO algorithm is that the potential solutions are quickened towards the best solutions. The simplified flow diagram is shown in Fig. 1.

The PSO algorithm starts with initializing each particle of the swarm by relegating an arbitrary speed and position in the issue seek space. The birds representing the particles or models, every particle has a location vector which represents the parameter value and a velocity vector. PSO characterizes a swarm of particles (models) in a M-dimensional space. Each particle keeps up memory of its past best position and velocity. At every iteration step, a velocity adjustment of the particle is resolved jointly by the previous best position which is called the T_{best} model occupied by the particle and the best position of the swarm. The new velocity is then used to compute a new position of the particle which is called the J_{best} model (Sen and Stoffa 2013). The update is described in the following equations (Sweilam et al. 2007):

$$\begin{aligned} V_i^{k+1} &= c_3 V_i^k + c_1 \text{rand}()\left(T_{best} - P_i^{k+1}\right) \\ &\quad + c_2 \text{rand}()\left[\left(J_{best} - P_i^{k+1}\right) P_i^{k+1}\right] \\ &= P_i^k + V_i^{k+1}, \end{aligned} \quad (3)$$

$$x_i^{k+1} = x_i^k + v_i^{k+1}. \quad (4)$$

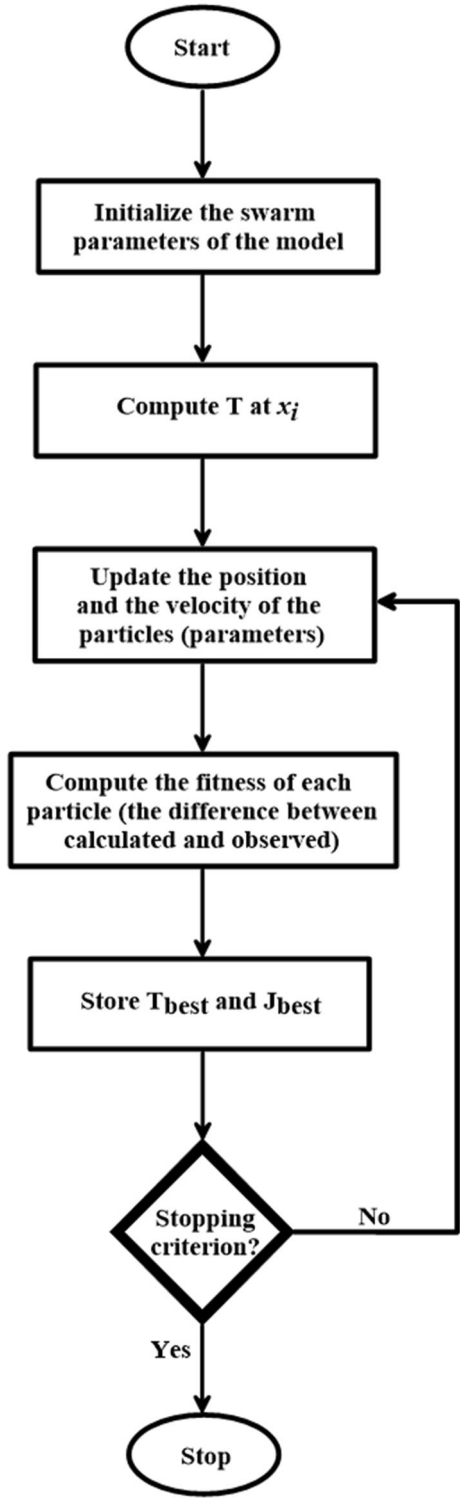

Figure 1
The work-flow of PSO algorithm applied to magnetic anomalies interpretation

where v_i^k is the velocity of the ith particle at the kth iteration, P_i^k is the current i model at the kth iteration, rand() is a uniform random number in the rang (0, 1). c_1 and c_2 are the positive consistent numbers which control the individual and the social behavior (Parsopoulos and Vrahatis 2002). c_3 is the inertial coefficient that control the particle velocity. x_i^k is the position of the particle i at the kth iteration. Thus, PSO has the main advantage of being very fast in executing the results and shows good balance between exploration and convergence.

The magnetic anomaly from Eq. 1 is calculated every iterative step for each x_i using the PSO algorithm. To estimate the quality of data fit at each iteration step of the inversion process, the RMS is defined as

$$\mathrm{RMS} = \sqrt{\frac{\sum_{i=1}^{N} [T_i^m(x_i) - T_i^c(x_i)]^2}{N}}. \qquad (5)$$

This is considered as the misfit between the observed and calculated anomalies.

2.4. Processing Time

In the present work, the real time for the entire computation process for a single model structure is almost 30 s for 100 models, while for 1000 model, the estimation process may reach from 8 to 12 min according to the number of iterations. However, for multiple structure models, the computation time increments to around 30%. The used code was developed using MS FORTRAN Developer studio in Window 7 on a simple desktop PC with Intel core i5 Processor.

3. Theoretical Examples

To illustrate the viability of the proposed inversion approach based on PSO algorithm, we have tested the PSO algorithm with three synthetic magnetic anomalies caused by simple geometrical shapes (a sphere, a horizontal cylinder, a thin sheet) without noise, tainted with different level of noise (5, 10, 15 and 20%) and multi-model example to investigate and evaluate whether the models obtained are close enough to the synthetic bodies.

3.1. Synthetic Noise-Free and Noisy Examples

The PSO technique was applied to noise-free synthetic magnetic anomalies due to a sphere model with K = 5000 nT, z = 7 m, θ = 50°, S_f = 2.5, x_o = 0 m, and profile length = 80 m, a horizontal cylinder model with K = 3000 nT, z = 11 m, θ = 35°, S_f = 2, x_o = 0 m, and profile length = 80 m and a thin sheet model with K = 1000 nT, z = 9 m, θ = − 30°, S_f = 1, x_o = 0 m, and profile length = 80 m. The magnetic field anomaly due to these models is computed from Eq. (1).

We started to test our method using 100 particles or models. The best model parameters were reached after 700 iterations, and the ranges of the parameters for sphere model (K from 3000 to 6000 nT, z from 1 to 12 m, θ from 5° to 90°, S_f from 0.2 to 3 and x_o from − 50 to 30 m), horizontal cylinder model (K from 1000 to 5000 nT, z from 1 to 16 m, θ from 5° to 90°, S_f from 0.2 to 3 and x_o from −50 to 30 m) and thin sheet model (K from 0 to 3000 nT, z from 1 to 16 m, θ from −50° to 60°, S_f from 0.2 to 3 and x_o from −50 to 30 m)models. The obtained results for each parameter (K, z, θ, S_f, x_o) are in a good and close agreement between exactly known and estimated model parameters, where the error percentages are equal to zero.

In addition, the three forward model anomalies for different source are also contaminated with random error of 5, 10, 15 and 20% (Figs. 2, 3, 4) to get magnetic anomalies as much as possible closer to the real ones and perceive the robustness of the PSO algorithm. The PSO algorithm was then adopted to estimate the model parameters (K, z, θ, S_f, x_o) of the simple geometrical shapes, utilizing Eq. (2) as the objective function. Initially, a suitable search range for each model parameters was selected as mentioned above and PSO was executed. Next, a PSO algorithm run was performed and the convergence of each model parameter and reduction of misfit (less RMS) were analyzed. PSO algorithm did not find the true depths, but it gave values close to the true depths.

The results of the proposed technique for sphere, horizontal cylinder and thin sheet models are mentioned in Figs. 2, 3, 4, respectively. According to the parameter values in the figures, the error in the estimated parameters and the RMS increase with increasing the noise on the magnetic field anomaly. In addition, the estimated model parameters do not vary too much, and it is realized that the PSO algorithm solution is not affected by the noise level. It can be observed that the results of model parameter estimation (K, z, θ, S_f, x_o) utilizing the PSO algorithm are attractive up to 20% of the random noise. Hence, this exhibits the stability of our newly presented method in light of the PSO algorithm.

3.2. Multi-Model Example

In this section, we produced and studied theoretically multi-model example generated and caused by multiple source bodies having different geometries and depths to test the effectiveness of the PSO algorithm on complicated anomalies.

We used the above-mentioned Eq. (1) to compute the magnetic anomaly (ΔT) for multi-synthetic model consisting of a sphere model with K = 11,000 nT, z = 4 m, θ = 30°, S_f = 2.5, x_o = 0 m, and profile length = 120 m and a horizontal cylinder model with K = 5000 nT, z = 6 m, θ = 40°, S_f = 2, x_o = 30 m, and profile length = 120 m and the magnetic anomaly is shown in Fig. 5.

The PSO algorithm was applied to the multi-model magnetic profile to appraise the distinctive model parameters in a way similar to the above-mentioned example.

However, in this case, all the structures were modeled altogether. The parameter ranges used as a part of the inversion process of the magnetic anomalies are presented in Table 1 together with the outcomes obtained for the model parameters. The inversion response (RMS of 7.4 nT) is contrasted with the data in Fig. 5. In addition, Fig. 5 shows the modeled magnetic anomaly and the subsurface structures considered for this model. It can be noticed that the parameters are quite well recuperated from the PSO algorithm.

4. Field Example

To test the validity of developed method on real cases, the PSO algorithm is connected to two field examples taken from the literatures. The results

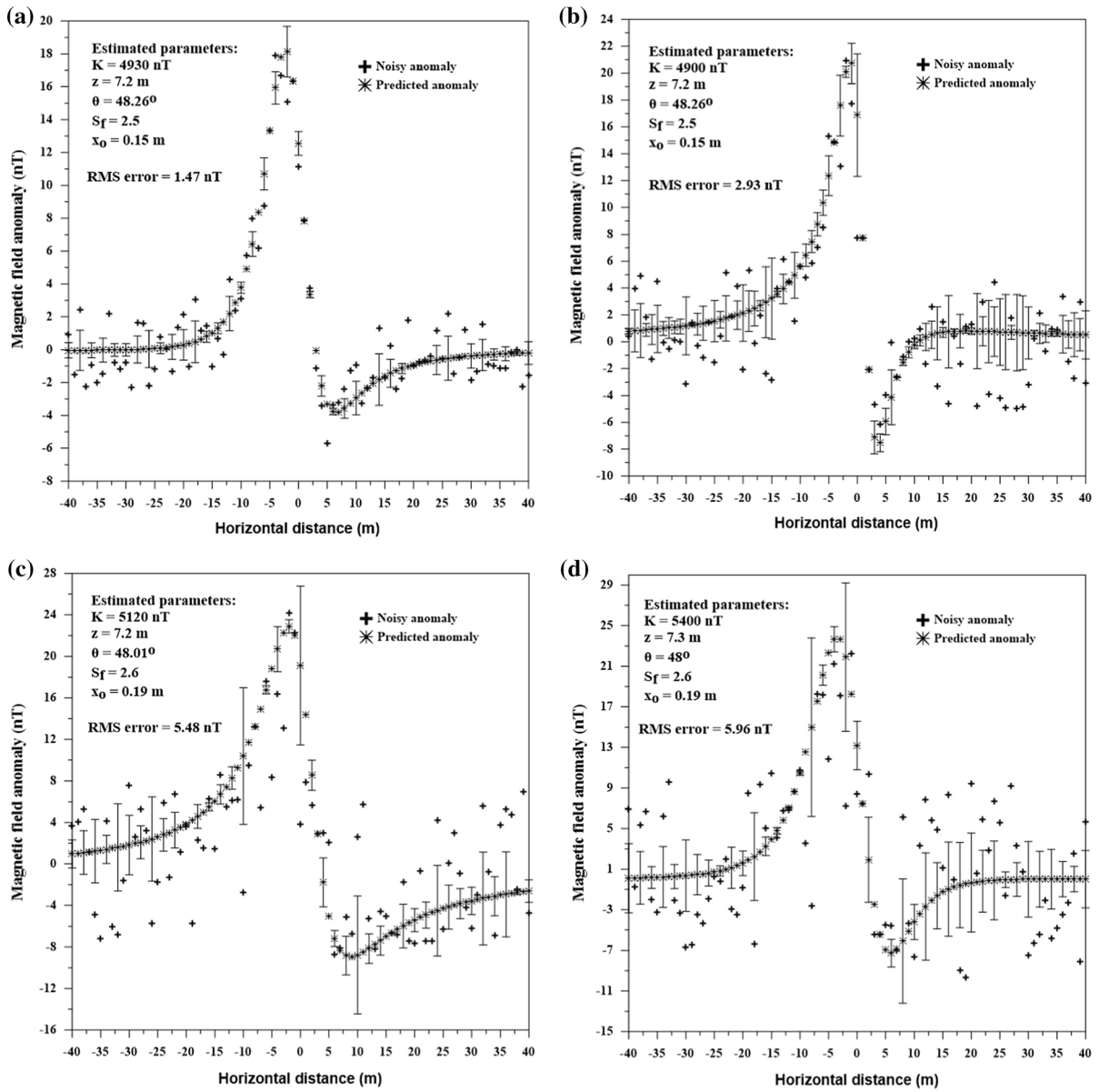

Figure 2
Noisy and predicted magnetic anomalies of a buried sphere-like geologic structure with K = 5000 nT, z = 7 m, θ = 50°, S_f = 2.5, x_o = 0 m, and profile length = 80 m, with **a** 5%, **b** 10%, **c** 15% and **d** 20% random noise. Error bars represents the standard deviations of the noise add to the noise-free datum

obtained by the proposed technique are compared with the results obtained from other inversion techniques. The two field examples that are utilized for testing the legitimacy of this technique are magnetic anomalies for Pima copper mine, USA and Hamrawein area, Egypt.

4.1. Pima Copper Mine Field Example, USA

The district of Pima mining is considered as one of the biggest porphyry copper in the nineteenth century. The mining area has delivered 4.36 billion pound of copper and other minerals like molybdenum, lead, silver and gold. Mineralization related

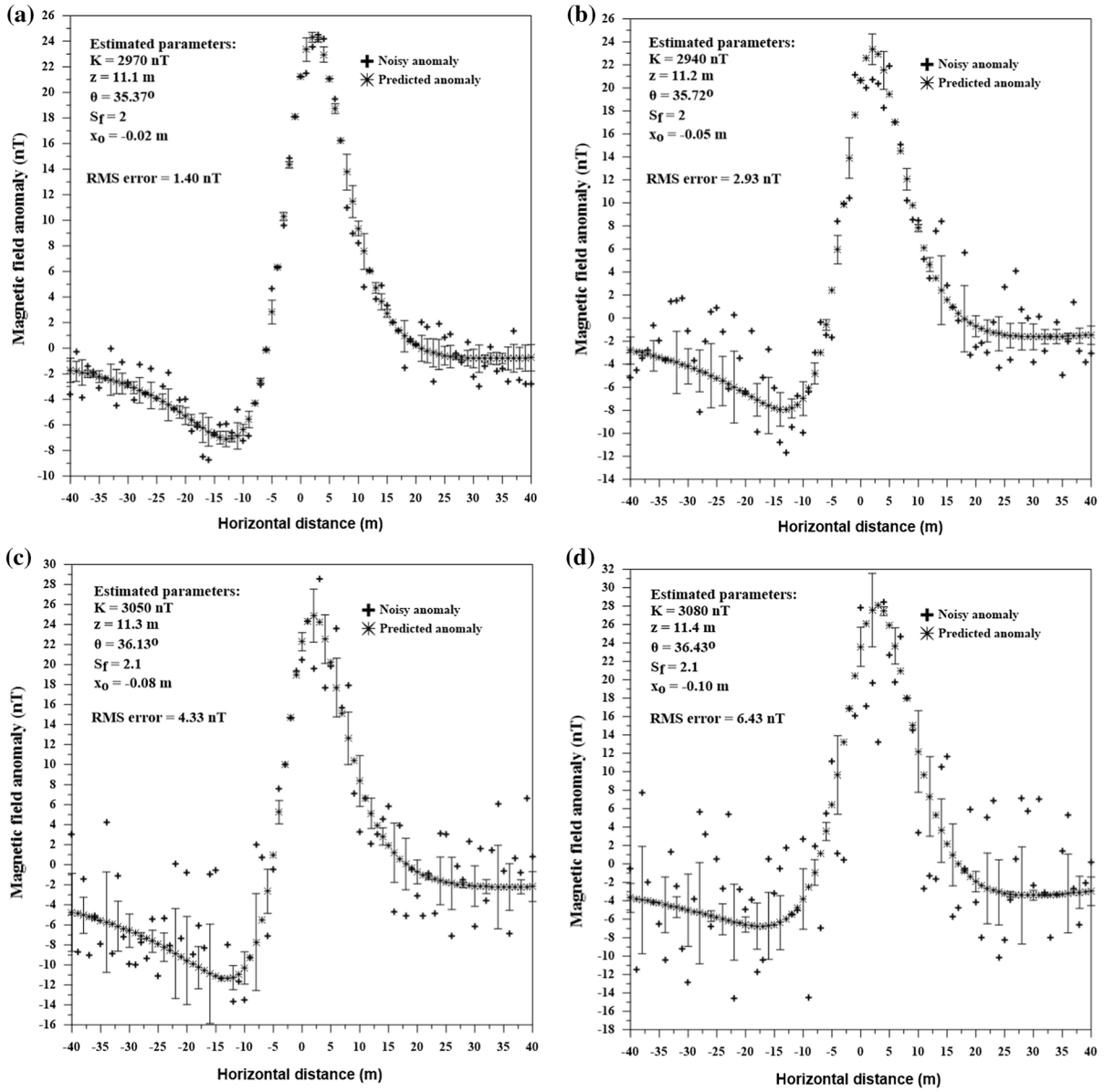

Figure 3
Noisy and predicted magnetic anomaly of a buried horizontal cylinder-like geologic structure with K = 3000 nT, z = 11 m, θ = 35°, S_f = 2, x_o = 0 m, and profile length = 80 m, with **a** 5%, **b** 10%, **c** 15% and **d** 20% random noise

with Laramide igneous activity was happened in Paleozoic sedimentary rocks, Mesozoic sedimentary and volcanic sequences, and in Paleocene igneous rocks. Post-mineralization, coarse-grained alluvial-clastic deposits accumulated in the fault contact with Precambrian to Paleocene rocks (Shafiqullah and Langlois 1978).

Figure 6 demonstrates the vertical component of magnetic anomaly profile over a thin sheet-like structure in Pima copper mine, Arizona, USA (Gay 1963). The profile length of 696 m was digitized at interim of 8.7 m. The ranges of the parameters utilized as a part of the method are presented in Table 2 which was picked regarding the accessible

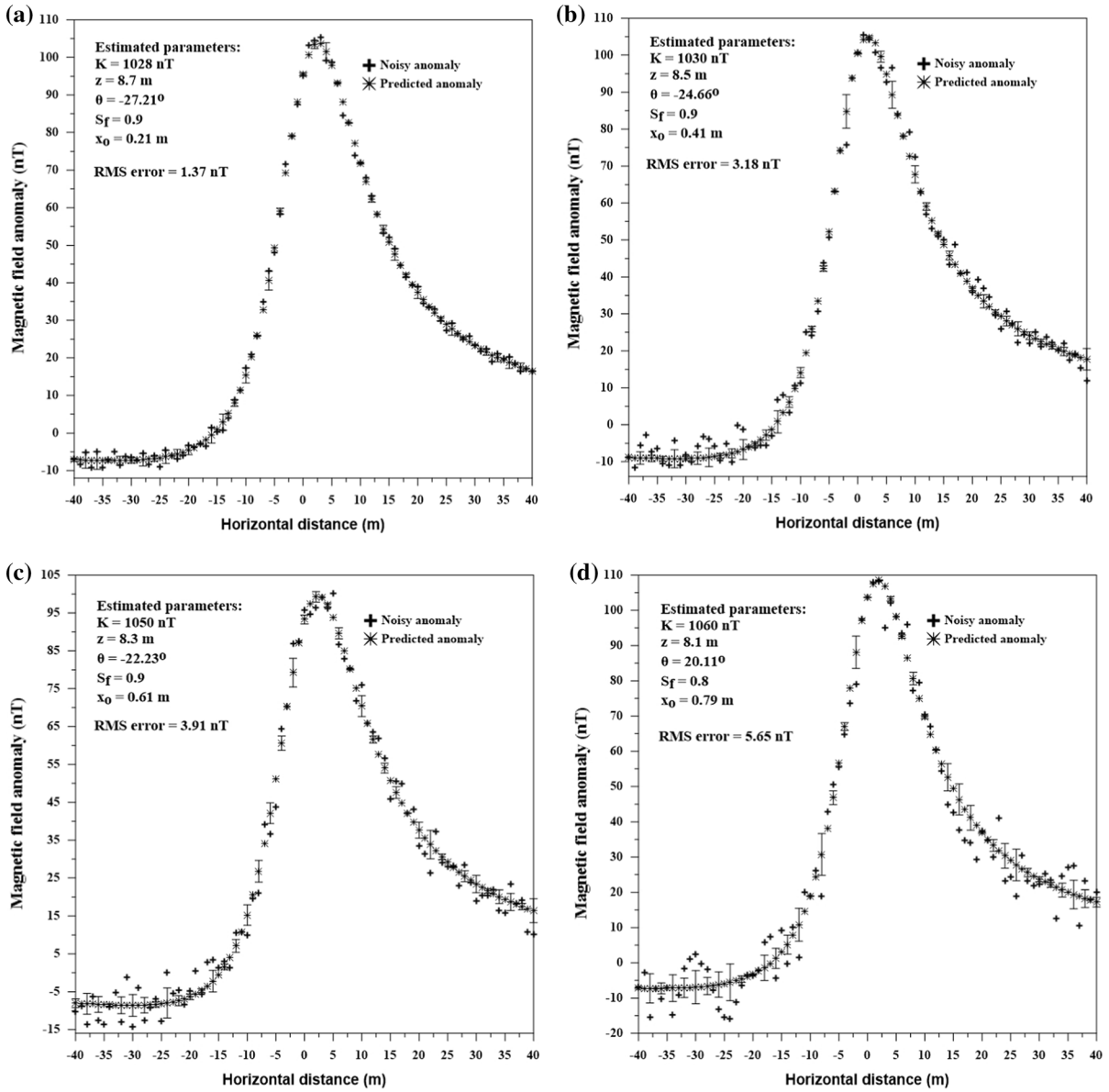

Figure 4
Noisy and predicted magnetic anomaly of a buried thin sheet-like geologic structure with K = 1000 nT, z = 9 m, $\theta = -30°$, S_f = 1, x_o = 0 m, and profile length = 80 m, with **a** 5%, **b** 10%, **c** 15% and **d** 20% random noise

geologic information. Table 2 demonstrates the assessed result of the model parameters (K = 600 nT, z = 71.08 m, $\theta = -47.83°$, S_f = 0.92, $x_o = -0.49$). The comparison between the measured and the predicted anomalies (Fig. 6) indicates the good agreement between them. The inverted parameters (K, z, θ, S_f) are found with a good correspondence with the drilling information and other information from published literatures (Gay 1963; Abdelrahman and Sharafeldin 1996) (Table 3). In addition, we compared our PSO approach results with very fast simulated annealing (VFSA) (Biswas et al. 2017) results (Table 3). This demonstrates that PSO approach has an execution time shorter (30 s) than VFSA approach.

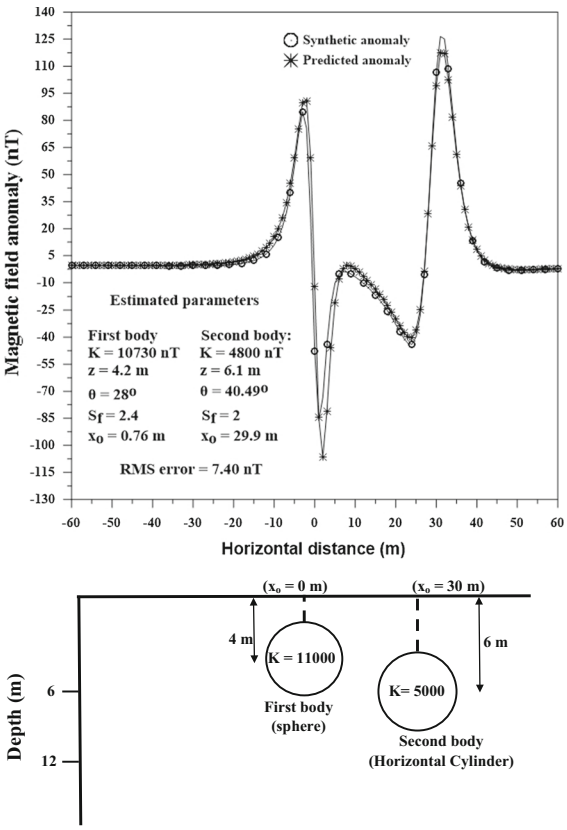

Figure 5
Synthetic and predicted magnetic anomalies of multi-model structure which consist of a sphere model with K = 11,000 nT, z = 4 m, θ = 30°, S_f = 2.5, x_o = 0 m, and profile length = 120 m and a horizontal cylinder model with K = 5000 nT, z = 6 m, θ = 40°, S_f = 2, x_o = 30 m, and profile length = 120 m

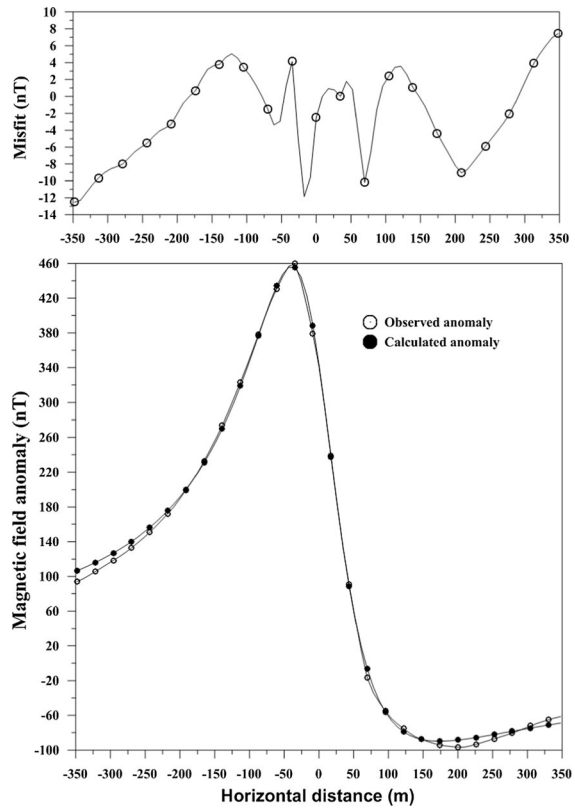

Figure 6
A vertical magnetic anomaly in Pima copper mine, USA (open circle) and the estimated magnetic anomaly (black circle) using PSO algorithm

4.2. *Hamrawein Area Field Example, Egypt*

The contextual investigation over the Hamrawein area, Egypt, is used for another magnetic data interpretation using the proposed PSO algorithm. The Hamrawein area is situated in the western edge of the Red Sea and spreads metavolcanic and sedimentary rocks (Salem 2005; Salem et al. 2005) (Fig. 7). The magnetic anomaly profile of 15,253.64 m has been taken from

Table 1

Numerical results for a multi-model theoretical example: spherical shape (K = 11,000 nT, z = 4 m, θ = 30°, S_f = 2.5, x_o = 0 m, and profile length = 120 m) and a horizontal cylinder (K = 5000 nT, z = 6 m, θ = 40°, S_f = 2, x_o = 30 m, and profile length = 120 m)

Type of body	Parameters	Used ranges	Result	Error (%)	RMS (nT)
Sphere	K (nT)	5000–12,000	10,730	2.4	7.40
	z (m)	2–8	4.2	7.5	
	θ (°)	10–45	28	6.66	
	S_f (dimensionless)	1–3	2.4	4	
	x_o (m)	− 20 to 10	0.76	–	
Horizontal cylinder	K (nT)	4000–8000	4800	4	
	z (m)	1–9	6.1	1.67	
	θ (°)	10–60	40.49	1.23	
	S_f (dimensionless)	1–3	2	0	
	x_o (m)	10–50	29.9	0.33	

Table 2

Numerical results for the vertical magnetic anomaly of the Pima copper mine field example, USA

Parameters	Used Ranges	Result	RMS (nT)
K (nT)	100–1500	610.12	4.52
z (m)	1–100	68.24	
θ (°)	− 90 to 90	− 49.46	
S_f (dimensionless)	0.2–3	0.92	
x_o (m)	− 696 to 174	− 0.49	

magnetic survey data which was led by Salem et al. (1999) (Fig. 8) and it was digitized at 214.844 m testing interval (Fig. 9). Table 4 shows the results of the inverted model parameters (depth, location of the origin, shape factor, index angle and the amplitude coefficient) over the Hamrawein area magnetic anomaly from the present method. It is seen from Fig. 9 that both predicted magnetic anomaly and observed magnetic anomaly curves are well correlated with the optimal RMS of

Table 3

Comparison between numerical results of different methods for the vertical magnetic anomaly of the Pima copper mine field example, USA

Method parameters	Gay method (1963)	Abdelrahman and Sharafeldin method (1996)	Asfahani and Tlas method (2007)	Tlas and Asfahani method (2011)	Tlas and Asfahani method (2015)	Biswas et al. method (2017)	Present method
K (nT)	–	596.50	577.60	576.82	666.15	613.0	610.12
z (m)	70.00	66.00	71.50	71.25	64.10	68.0	68.24
θ (°)	− 50.00	− 53.00	− 50.50	− 47.58	− 44.70	–	− 49.46
S_f		(dimensionless)	–	–	–	–	–
1.0 (fixed)	0.92						
x_o (m)	–	–	–	− 0.22	–	− 4.3	− 0.49

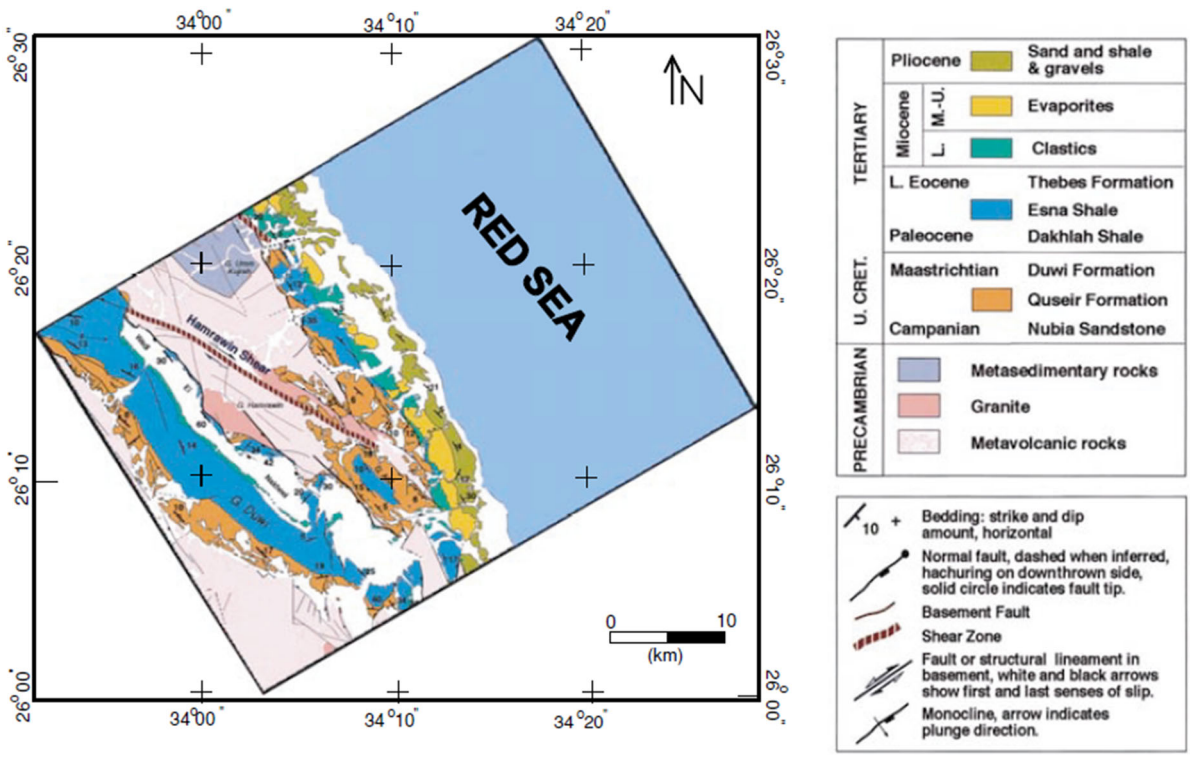

Figure 7
Geological map of the Hamrawein field example, Quseir area, northern Red Sea, Egypt (Salem et al. 2005)

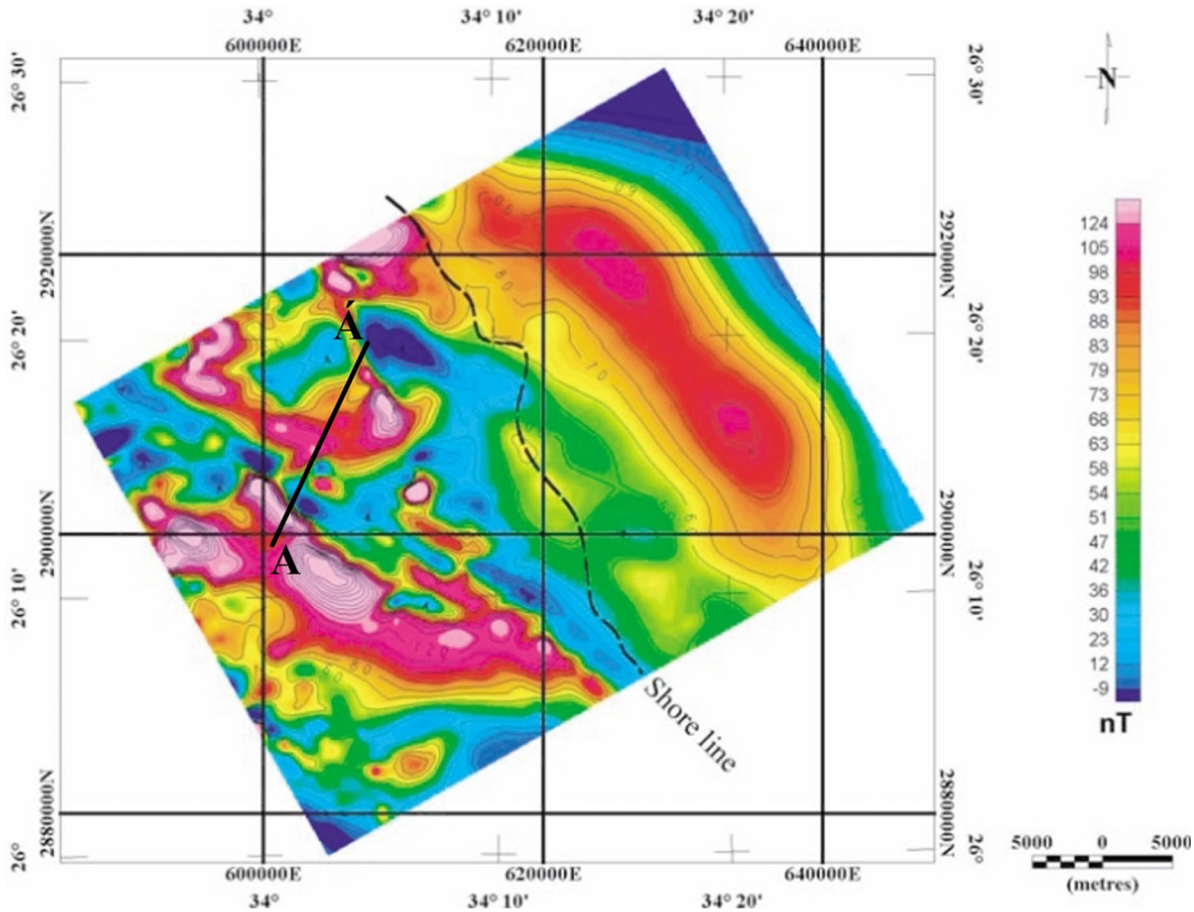

Figure 8
Total magnetic intensity map of the Hamrawein field example, Quseir area, northern Red Sea, Egypt (Salem et al. 2005)

15.97 nT. The optimum results of the model parameters (K, z, θ, S_f, x_o) are $K = 507.64$ nT, $z = 601.56$ m, $\theta = 57.04°$, $S_f = 0.89$, $x_o = 4255.98$ m for the first anomaly, while the parameters of the second anomaly are $K = 427.38$ nT, $z = 515.62$ m, $\theta = 37.27°$, $S_f = 0.93$, $x_o = 14{,}823.69$ m, respectively. From the above results ($S_f = 0.89$ and 0.93) we can reason that the two magnetic anomalies are caused by thin sheets. The correlation between the results obtained from our method and that published in the literature is shown in Table 5.

5. Conclusions

In this investigation, we have represented the applicability and the stability of the PSO algorithm (particle swarm optimization) in estimating the distinctive body parameters (K, z, θ, x_o, S_f) for various synthetic and real examples. The PSO algorithm has been applied for magnetic anomalies of assuming models, for example, simple bodies (spheres, horizontal cylinders and thin sheets). This technique has been verified and demonstrated on synthetic magnetic anomalies with and without random noise, multi-models and lastly connected to two field examples from USA and Egypt. The evaluated results revealed that this approach is steady, powerful and proficient in tackling such a magnetic problem and solving the quantitative interpretation of magnetic data when comparing it with the results published in the state-of-arts. This technique is not independent on promising initial models. Furthermore, the

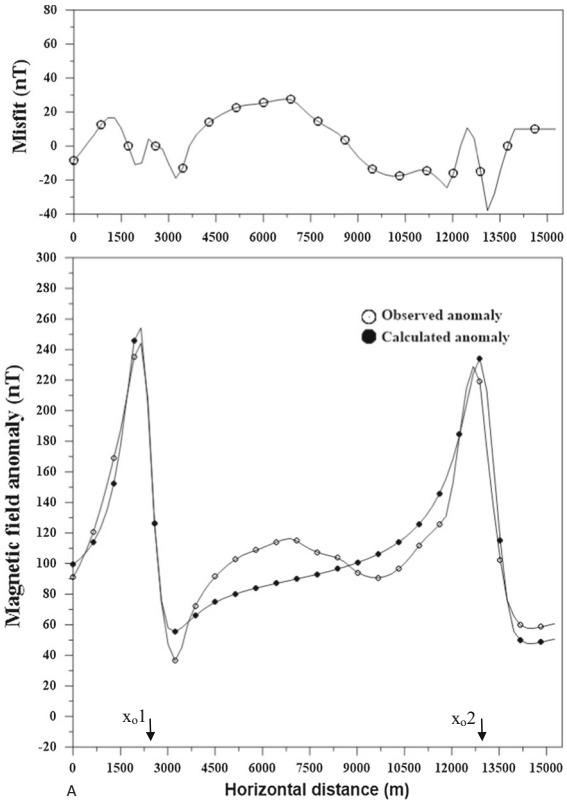

Figure 9
Total magnetic anomaly profile (A–Á) over the Hamrawein area, on the western margin of the Red Sea, Egypt (open circle) and the estimated magnetic anomaly (black circle) using PSO algorithm

Table 4

Numerical results for magnetic anomaly over the Hamrawein area, on the western margin of the Red Sea, Egypt

Parameters	Used ranges	Result	RMS (nT)
First anomaly			
K (nT)	0–5000	507.64	14.76
z (m)	100–1500	623.05	
θ (°)	− 90–90	57.04	
S_f (dimensionless)	0.7–2.5	0.89	
x_o (m)	3860–5371	4255.98	
Second anomaly			
K (nT)	0–5000	427.38	
z (m)	100–1500	494.14	
θ (°)	− 90 to 90	37.27	
S_f (dimensionless)	0.7–2.5	0.93	
x_o (m)	13,964–16,113	14,823.96	

convergence to the best estimation of the inverted model parameters of the buried structure is quickly reached. This new methodology to invert 2D magnetic data is recommended for quick analysis of magnetic anomaly profiles in an attempt to estimate the best inverted model parameter values related to different bodies such as sphere, horizontal cylinder, and thin sheet-like geologic structures. In addition, the PSO outcomes could be of importance for a gradient-descent method as an initial model.

Table 5

Comparison between the numerical results of different methods for magnetic anomaly over the Hamrawein area, on the western margin of the Red Sea, Egypt

Method parameters	Salem et al. method (2005)	Salem method (2005)	Present method
First anomaly			
K (nT)	–	–	507.64
z (m)	555.7 ± 10 m	540 ± 30 m	623.05
θ (°)	–	–	57.04
S_f	(dimensionless)	–	–
0.89			
x_o (m)	4526.3 ± 7 m	4530 ± 10 m	4255.98
Second anomaly			
K (nT)	–	–	427.38
z (m)	441.2 ± 13 m	477 ± 25 m	494.14
θ (°)	–	–	37.27
S_f	(dimensionless)	–	–
0.93			
x_o (m)	14,858.4 ± 17 m	14,850 ± 21 m	14,823.96

Acknowledgements

Authors would like to thank Prof. A. Rabinovich; C. Braitenberg; R. Dmowska Editors-in-Chief, Prof. Dr. Colin Farquharson, the Editor, Prof. Rodrigo Bijani, reviewer, and the other capable reviewer for their constructive comments for enhancing our original manuscript. Thanks are also due to Prof. Salah Mehanee, Geophysics Department, Faculty of Science, Cairo University, for his help and constant encouragement.

References

Abdelrahman, E. M., Abo-ezz, E. R., & Essa, K. S. (2012). Parametric inversion of residual magnetic anomalies due to simple geometric bodies. *Exploration Geophysics, 43,* 178–189.

Abdelrahman, E. M., Abo-Ezz, E. R., Essa, K. S., El-Araby, T. M., & Soliman, K. S. (2007). A new least-squares minimization approach to depth and shape determination from magnetic data. *Geophysical Prospecting, 55,* 433–446.

Abdelrahman, E. M., El-Araby, H. M., El-Araby, T. M., & Essa, K. S. (2003). A least-squares minimization approach to depth determination from magnetic data. *Pure and Applied Geophysics, 160,* 1259–1271.

Abdelrahman, E. M., & Essa, K. S. (2005). Magnetic interpretation using a least-squares, depth-shape curves method. *Geophysics, 70,* L23–L30.

Abdelrahman, E. M., & Essa, K. S. (2015). A new method for depth and shape determinations from magnetic data. *Pure and Applied Geophysics, 172,* 439–460.

Abdelrahman, E. M., Essa, K. S., El-Araby, T., & Abo-Ezz, E. R. (2016). Depth and shape solutions from second moving average residual magnetic anomalies. *Exploration Geophysics, 47,* 58–66.

Abdelrahman, E. M., & Sharafeldin, S. M. (1996). An iterative least-squares approach to depth determination from residual magnetic anomalies due to thin dikes. *Journal of Applied Geophysics, 34,* 213–220.

Abdelrahman, E. M., Soliman, K. S., El-Araby, T. M., Abo-Ezz, E. R., & Essa, K. S. (2009). A least-squares standard deviation method to interpret magnetic anomalies due to thin dikes. *Near Surface Geophysics, 7,* 41–46.

Abedi, M., Gholami, A., & Norouzi, G. H. (2013). A stable downward continuation of airborne magnetic data: A case study for mineral prospectivity mapping in Central Iran. *Computers and Geosciences, 52,* 269–280.

Abo-Ezz, E. R., & Essa, K. S. (2016). A least-squares minimization approach for model parameters estimate by using a new magnetic anomaly formula. *Pure and Applied Geophysics, 173,* 1265–1278.

Abubakar, R., Muxworthy, A. R., Sephton, M. A., Southern, P., Watson, J. S., Fraser, A. J., et al. (2015). Formation of magnetic minerals at hydrocarbon-generation conditions. *Marine and Petroleum Geology, 68,* 509–519.

Al-Garni, M. A. (2011). Magnetic and DC resistivity investigation for groundwater in a complex subsurface terrain. *Arabian Journal of Geosciences, 4,* 385–400.

Araffa, S. A. S., Helaly, A. S., Khozium, A., Lala, A. M. S., Soliman, S. A., & Hassan, N. M. (2015). Delineating groundwater and subsurface structures by using 2D resistivity, gravity and 3D magnetic data interpretation around Cairo-Belbies Desert road, Egypt. *NRIAG Journal of Astronomy and Geophysics, 4,* 134–146.

Asfahani, J., & Tlas, M. (2007). A robust nonlinear inversion for the interpretation of magnetic anomalies caused by faults, thin dikes and spheres like structure using stochastic algorithms. *Pure and Applied Geophysics, 164,* 2023–2042.

Balkaya, C., Ekinci, Y. L., Göktürkler, G., & Turan, S. (2017). 3D non-linear inversion of magnetic anomalies caused by prismatic bodies using differential evolution algorithm. *Journal of Applied Geophysics, 136,* 372–386.

Bektas, Ö., Ravat, D., Büyüksaraç, A., Bilim, F., & Ateş, A. (2007). Regional geothermal characterisation of East Anatolia from aeromagnetic, heat flow and gravity data. *Pure and Applied Geophysics, 164,* 976–986.

Biswas, A. (2015). Interpretation of residual gravity anomaly caused by a simple shaped body using very fast simulated annealing global optimization. *Geoscience Frontiers, 6,* 875–893.

Biswas, A., Parija, M. P., & Kumar, S. (2017). Global nonlinear optimization for the interpretation of source parameters from total gradient of gravity and magnetic anomalies caused by thin dyke. *Annals of Geophysics, 60*(2), G0218.

Boschetti, F., Denith, M. C., & List, R. D. (1997). Inversion of potential field data by genetic algorithms. *Geophysical Prospecting, 45,* 461–478.

Bresco, M., Raiconi, G., Barone, F., DeRosa, R., & Milano, L. (2005). Genetic approach helps to speed classical Price algorithm for global optimization. *Soft Computing, 9,* 525–535.

Cedeno, W., & Agrafiotis, D. K. (2003). Using particle swarms for the development of QSAR models based on K-nearest neighbor and kernel regression. *Journal of Computer Aided Molecular Design, 17,* 255–263.

Chau, W. K. (2008). Application of a particle swarm optimization algorithm to hydrological problems. In L. N. Robinson (Ed.), *Water Resources Research Progress* (pp. 3–12). New York: Nova Science Publishers Inc.

Colorni, A., Dorigo, M., & Maniezzo, V. (1991). Distributed optimization by ant colonies. In *Proceedings of the 1st European conference on artificial life* (pp. 134–142).

Davis, K., Yaoguo Li, Y., & Nabighian, M. (2010). Automatic detection of UXO magnetic anomalies using extended Euler deconvolution. *Geophysics, 75*(3), G13–G20.

Di Maio, R., Rani, P., Piegari, E., & Milano, L. (2016). Self-potential data inversion through a genetic-price algorithm. *Computers and Geosciences, 94,* 86–95.

Donelli, M., Franceschini, G., Martini, A., & Mass, A. (2006). An integrated multiscaling strategy based on a particle swarm algorithm for inverse scattering problems. *IEEE Transactions on Geoscience and Remote Sensing, 44,* 298–312.

Dong, P., Fan, J. L., Liu, C. H., Chen, G. W., Wang, L. S., Sun, B., et al. (2007). Magnetic anomaly characteristics out of reinforcement cage in cast-in situ pile. *Progress in Geophysics, 22*(5), 1660–1665. **(in Chinese)**.

Eberhart, R. C., & Shi, Y. (2001). Particle swarm optimization: Developments, applications and resources. In *Proceedings of the congress on evolutionary computation, Seoul, Korea* (pp. 81–86).

Ekinci, Y. L., Balkaya, Ç., Göktürkler, G., & Turan, S. (2016). Model parameter estimations from residual gravity anomalies due to simple-shaped sources using differential evolution algorithm. *Journal of Applied Geophysics, 129,* 133–147.

Ekinci, Y. L., Balkaya, Ç., Şeren, A., Kaya, M. A., & Lightfoot, C. S. (2014). Geomagnetic and geoelectrical prospection for buried archaeological remains on the Upper City of Amorium, a Byzantine City in Midwestern Turkey. *Journal of Geophysics and Engineering, 11,* 015012.

Essa, K. S., & Elhussein, M. (2017a). A new approach for the interpretation of magnetic data by a 2-D dipping dike. *Journal of Applied Geophysics, 136,* 431–443.

Essa, K. S., & Elhussein, M. (2017b). 2D dipping dike magnetic data interpretation using a robust particle swarm optimization. *Geoscientific Instrumentation, Methods and Data Systems, Discuss.*. https://doi.org/10.5194/gi-2017-39.

Farquharson, C. G., & Craven, J. A. (2009). Three-dimensional inversion of magnetotelluric data for mineral exploration: An example from the McArthur River uranium deposit, Saskatchewan, Canada. *Journal of Applied Geophysics, 68,* 450–458.

Fedi, M. (2007). DEXP: A fast method to determine the depth and the structural index of potential fields sources. *Geophysics, 72,* I1–I11.

Gay, P. (1963). Standard curves for interpretation of magnetic anomalies over long tabular bodies. *Geophysics, 28,* 161–200.

Gay, P. (1965). Standard curves for the interpretation of magnetic anomalies over long horizontal cylinders. *Geophysics, 30,* 818–828.

Gündoğdu, N. Y., Candansayar, M. E., & Genç, E. (2017). Rescue archaeology application: Investigation of Kuriki mound archaeological area (Batman, SE Turkey) by using direct current resistivity and magnetic methods. *JEEG, 22*(2), 177–189.

He, J., & Guo, H. (2013). A modified particle swarm optimization algorithm. *Telkomnika, 11*(10), 6209–6215.

Ivakhnenkoa, O. P., Abirova, R., & Logvinenkoc, A. (2015). New method for characterisation of petroleum reservoir fluid mineral deposits using magnetic analysis. *Energy Procedia, 76,* 454–462.

Juang, C. F. (2004). A hybrid genetic algorithm and particle swarm optimization for recurrent network design. *IEEE Transactions on Systems, Man, and Cybernetics, Part B, 34,* 997–1006.

Kaftan, I. (2017). Interpretation of magnetic anomalies using a genetic algorithm. *Acta Geophysica, 65,* 627–634.

Kennedy, J., & Eberhart, R. (1995). Particle Swarm Optimization. In *IEEE international conference on neural networks (Perth, Australia): IEEE Service Center, PiscatawaY, NJ, lV* (pp. 1942–1948).

Ku, C. C., & Sharp, J. A. (1983). Werner deconvolution for automated magnetic interpretation and its refinement using Marquardt's inverse modeling. *Geophysics, 48,* 754–774.

Lines, L. R., & Treitel, S. (1984). A review of least-squares inversion and its application to geophysical problems. *Geophysical Prospecting, 32,* 159–186.

Mehanee, S. (2014). Accurate and efficient regularized inversion approach for the interpretation of isolated gravity anomalies. *Pure and Applied Geophysics, 171,* 1897–1937.

Mehanee, S., & Essa, K. S. (2015). 2.5D regularized inversion for the interpretation of residual gravity data by a dipping thin sheet: Numerical examples and case studies with an insight on sensitivity and non-uniqueness. *Earth Planets Space, 67,* 130.

Mehanee, S., Essa, K. S., & Smith, P. D. (2011). A rapid technique for estimating the depth and width of a two-dimensional plate from self-potential data. *Journal of Geophysics and Engineering, 8,* 447–456.

Nabighian, M. N., Grauch, V. J. S., Hansen, R. O., LaFehr, T. R., Li, Y., Peirce, J. W., et al. (2005). The historical development of the magnetic method in exploration. *Geophysics, 70*(6), 33–61.

Nyabeze, P. K., & Gwavava, O. (2016). Investigating heat and magnetic source depths in the Soutpansberg Basin, South Africa: Exploring the Soutpansberg Basin Geothermal Field. *Geothermal Energy, 4,* 8.

Pallero, J. L. G., Fernández-Muñiz, M. Z., Cernea, A., Álvarez-Machancoses, Ó., Pedruelo-González, L. M., Bonvalot, S., et al. (2018). Particle swarm optimization and uncertainty assessment in inverse problems. *Entropy, 20*(2), 96.

Parsopoulos, K. E., & Vrahatis, M. N. (2002). Recent approaches to global optimization problems through particle swarm optimization. *Natural Computing, 1,* 235–306.

Peksen, E., Yas, T., & Kıyak, A. (2014). 1-D DC resistivity modeling and interpretation in anisotropic media using particle swarm optimization. *Pure and Applied Geophysics, 171*(9), 2371–2389.

Pilkington, M. (2006). Joint inversion of gravity and magnetic data for two-layer models. *Geophysics, 71,* L35–L42.

Rao, B. S. R., Murthy, I. V. R., & Rao, C. V. (1973). A computer program for interpreting vertical magnetic anomalies of spheres and horizontal cylinders. *Pure and Applied Geophysics*, *110*, 2056–2065.

Rao, B. S. R., Rao, T. K. S. P., & Murthy, A. S. K. (1977). A note on magnetized spheres. *Geophysical Prospecting, 25,* 746–757.

Rao, T., & Subrahmanyam, M. (1988). Characteristic curves for the inversion of magnetic-anomalies of spherical ore bodies. *Pure and Applied Geophysics, 126,* 69–83.

Rao, T. K. S. P., Subrahmanyam, M., & Srikrishna Murthy, A. (1986). Nomograms for the direct interpretation of magnetic anomalies due to long horizontal cylinders. *Geophysics, 51,* 2156–2159.

Robinson, J., & Rahamat-Samii, Y. (2004). Particle swarm optimization in electromagnetic. *IEEE Transactions on Antennas and Propagation, 52,* 397–407.

Salem, A. (2005). Interpretation of magnetic data using analytic signal derivatives. *Geophysical Prospecting, 53,* 75–82.

Salem, A., Aboud, E., Elsirafy, A., & Ushijima, K. (2005). Structural mapping of Quseir area, northern Red Sea, Egypt, using high-resolution aeromagnetic data. *Earth, Planets and Space, 57,* 761–765.

Salem, A., Elsirafi, A., & Ushijima, K. (1999). Design and application of high-resolution aeromagnetic survey over Gebel Duwi area and its offshore extension, Egypt. *Memoirs of the Faculty of Engineering, Kyushu University, 59,* 201–213.

Sen, M. K., & Stoffa, P. L. (2013). *Global optimization methods in geophysical inversion* (p. 279). Cambridge: Cambridge University Press.

Shafiqullah, M., & Langlois, J. D. (1978). The Pima mining district Arizona—A geochronologic update. In *New Mexico geological society guidebook 29th annual fall field conference guidebook* (pp. 321–327).

Singh, A., & Biswas, A. (2016). Application of global particle swarm optimization for inversion of residual gravity anomalies over geological bodies with idealized geometries. *Natural Resources Research, 25*(3), 297–314.

Srivastava, S., Datta, D., Agarwal, B. N. P., & Mehta, S. (2014). Applications of ant colony optimization in determination of source parameters from total gradient of potential fields. *Near Surface Geophysics, 12,* 373–389.

Sweilam, N. H., El-Metwally, K., & Abdelazeem, M. (2007). Self potential signal inversion to simple polarized bodies using the particle swarm optimization method: A visibility study. *Journal of Applied Geophysics, 6,* 195–208.

Tarantola, A. (2005). *Inverse problem theory and methods for model parameter estimation*. Philadelphia: Society for Industrial and Applied Mathematics (SIAM)

Thompson, D. T. (1982). EULDPH—A new technique for making computer-assisted depth estimates from magnetic data. *Geophysics, 47,* 31–37.

Tlas, M., & Asfahani, J. (2011). Fair function minimization for interpretation of magnetic anomalies due to thin dikes, spheres and faults. *Journal of Applied Geophysics, 75,* 237–243.

Tlas, M., & Asfahani, J. (2015). The simplex algorithm for best-estimate of magnetic parameters related to simple geometric-shaped structures. *Mathematical Geosciences, 47,* 301–316.

Toushmalani, R. (2013). Gravity inversion of a fault by particle swarm optimization (PSO). *Springer Plus, 2,* 315.

van den Bergh, F., & Engelbrecht, A. P. (2004). A Cooperative approach to particle swarm optimization. *IEEE Transactions on Evolutionary Computation, 8,* 225–239.

Wachowiak, M. P., Smolıkova, R., Zheng, Y., Zurada, J. M., & Elmaghraby, A. S. (2004). An approach to multimodal biomedical image registration utilizing particle swarm optimization. *IEEE Transactions on Evolutionary Computation, 8,* 289–301.

Yin, G., Zhang, Y., Fan, H., Ren, G., & Li, Z. (2017). Automatic detection of multiple UXO-like targets using magnetic anomaly inversion and self-adaptive fuzzy c-means clustering. *Exploration Geophysics, 48*(1), 67–75.

Zhdanov, M. S. (2002). *Geophysical inversion theory and regularization problems* (p. 633). Amsterdam: Elsevier.

(Received April 21, 2017, revised March 28, 2018, accepted April 9, 2018, Published online April 19, 2018)